Chapter V

In situ structure of the complete *Hylemonella gracilis* flagellar motor

Gavin E. Murphy[1], Eric G. Matson[2], Jared R. Leadbetter[2], Grant J. Jensen[1*]

Divisions of Biology[1] and Environmental Science and Engineering[2]

California Institute of Technology, Pasadena, CA 91125

*To whom correspondence should be addressed: 1200 E. California Blvd., Pasadena, CA 91125, 626-395-8827 (phone), 626-395-5730 (fax), Jensen@caltech.edu.

Abstract

The bacterial flagellar motor is an amazing nanomachine: Built from about 25 different proteins, it uses an electrochemical ion gradient to drive rotation at speeds normally around 60 Hz[1-3] in *E. coli.* The flagellar motor consists of a fixed, membrane-embedded, torque-generating stator and a typically bidirectional, spinning rotor that changes direction in response to chemotactic signals. While previous structural work has targeted the purified rotor from proteobacteria[4-6] or the *in situ* spirochete flagellar motor[7], little is known about the more typical stator from extracellular flagellar motors. Using electron cryotomography of whole cells, here we show the *in situ* structure of the complete flagellar motor from the betaproteobacteria *Hylemonella gracilis* at 6.5 nm resolution. Fifty-nine individual motor particles were computationally extracted from the reconstructions, aligned, and then averaged. The stator assembly possessed 11-, 12-, and 13-fold symmetry; lay next to the rotor; and was connected directly to the C ring. The stator studs were as large as the expected volume of two OmpA domains. Two novel structures were observed: an extended E collar around the P ring, and a transport (TA) ring under the rotor.

Introduction

The bacterial flagellar motor excites considerable interest because of the ordered expression of its genes, its regulated self-assembly, the complex interactions of its many proteins, and its startling mechanical abilities. Stator proteins MotA and MotB form a ring of "studs" within and above the inner membrane that couple the passage of protons across the membrane to the generation of torque[1, 2]. Above the membrane, MotB has a

peptidoglycan-binding domain that presumably holds the stator in place by binding to the globally cross-linked peptidoglycan layer[1, 2]. Below the membrane, the cytoplasmic loops of MotA are believed to spin a wheel of FliG molecules, which like radial spokes extend roughly parallel to the membrane from the rotor in the middle to just below MotA on the periphery[1]. Proteinaceous P and L rings serve as bearings to facilitate the rotation of the rod within the peptidoglycan and outer membranes, respectively[1, 2]. Inside the cell and below FliG lies the C ring, which regulates the direction of rotation in response to the chemotactic system[1, 2].

Flagellar basal bodies containing the rotor, rod, and sometimes the C ring have been purified and reconstructed by electron cryomicroscopy-based single particle analysis[4, 8, 9]. The *Salmonella* rotor possessed a mean symmetry of 25[6] or 26[10] while its C ring possessed a mean symmetry of 34[6, 11]. Because the stators do not co-purify with the rotor, however, little is known about *Salmonella*'s stator structure and interactions with the rest of the motor. Patterns of stator studs have been seen in 2D, freeze-etch images, but the interpretation of these images is difficult and the maximum number of studs has been reported as either 12 or 16, depending on the species[12-15]. For the former group, the number of studs ranged between 10 and 12. *T. primitia* had 16 studs, whose volumes were each twenty times larger than MotB's 2 OmpA domains[7]. The number of torque-generating units has been reported as either 8 or at least 11[2, 3, 16]. 2-D cryo-EM images of purified PomA/PomB complexes (homologs of MotA and MotB) from *V. alginolyticus* have revealed an ~ 70 Å long, thin extension above the membrane[17].

Results and Discussion

Here we report the complete structure of the *Hylemonella gracilis* flagellar motor obtained by electron cryotomography. *H. gracilis* was chosen because it is 250 nm wide and is a bipolar, lophotrichous spirillum with one to four flagella per tip, which maximizes the number of motors per reconstruction. It is also a betaproteobacteria and so is more related to the motors of the gammaproteobacteria *Salmonella* and *E. coli* than *T. primitia* is. Fifteen tomographic reconstructions were made from tilt-series of cells that were frozen in vitreous ice (Fig. V-1). The cell had flagellar motors, probable chemotaxis receptor arrays, a ribosome-free region that may be the nucleoid, ribosome-like particles and oddly, some cells had flagella-like filaments mistakenly located in their cytoplasm (Fig. V-1). The tilt-series were CTF corrected[18] (see Supp. Fig. V-S1), but no improvement in the resolution of the final structure was detected compared to uncorrected reconstructions. From the tomograms, fifty-nine flagellar motor particles were computationally extracted, aligned, and averaged (Fig. V-2). In some individual particles, symmetry elements were visible (Fig. V-2a), but clearer results emerged from the average (Fig. V-2e).

Several components of the individual, aligned particles were tested for rotational symmetry. With one method, the rotational correlation of 3-D volumes containing the motor components was calculated in real-space, and in their averaged 1-D power spectrum, only 13-fold symmetry was detected and only in the stator regions both above and below the inner membrane (See Supplementary Fig. V-2a). The symmetry of the other components was presumably undetectable because of the low resolution. The

average of all particles was thus 13-fold symmetrized (Fig. V-2f). The isosurface of this final "homogenous" structure is shown in Fig. V-3. The contour plot of the homogeneous motor and its 99% confidence interval is shown in Supp. Fig. V-S5 and V-S6. At the lower limit, the stator studs and stator connection regions disappear, so they have lower significance than other features.

Using the program ROTASTAT[19], the rotational correlation of individual 2-D images made by binning 3-D volumes in z was calculated in reciprocal space and judged for statistical significance. 11-, 12-, and 13-fold symmetry was detected with significance in the stator stud region above and in the membrane, and 12- and 13-fold symmetry was detected in the stator connections region below the membrane. The particles displaying strong symmetry were classified according to their stator symmetry. The 1-D power spectrum of the three symmetry classes and the unclassified group is shown in Supplementary Fig. V-2b. 13-fold symmetry appears to be dominant. The strongly 12-fold and 13-fold symmetric classes were then separately aligned, averaged, and symmetrized accordingly. The 12-fold class had eighteen members and the 13-fold class fifteen. The separate averages and symmetrized averages are shown in Supp. Fig. V-S3. The 13-fold class had more contrast-rich stator symmetry elements than the 12-fold group (cf. slices 8 and 9 in each panel of Supp. Fig. V-S3). The isosurfaces of the two "heterogeneous" final structures are shown in Supp. Fig. V-S4. In line with recent functional studies[3], the stator symmetry was at least 11. 8-fold symmetry was not detected.

The final, homogeneous, *H. gracilis* structure has thirteen studs emerging from its stator region (marked S in Fig. V-3b) that each fill a volume expected for the two OmpA domains of the two MotB proteins, unlike *T. primitia*, whose sixteen stator studs were each twenty times larger[7]. The separate 13-fold class also has prominent stator stud density that resembles the homogeneous structure, but the studs of the 12-fold class do not extend much from the membrane (Supp. Fig. V-S4). Either the 12-fold class happens to lack density, or perhaps they are truly 13-fold but have been misclassified because of low contrast. Henceforth, the homogeneous structure will be the focus. The studs extend ~ 8 nm from the membrane (Fig. V-4c), which is similar to the 7 nm length seen with *Vibrio alginolyticus* stators embedded in liposomes[17]. The center-to-center diameter of the studs above the IM is ~ 48–51 nm and the diameter of the stator connections below the IM is 42 nm, so the stators lean out ~ 16º from the center axis. The central arc length per stator is ~ 12 nm, which is large enough to accommodate the predicted dimensions of one $(MotA)_4(MotB)_2$ stator unit[20]. The center-to-center diameter of the 12-fold studs has nearly identical dimensions. The studs are right above the stator connection density (bridging density #1 in Fig. V-3b) and do not lean CCW like *T. primitia*'s[7].

The stators interact with the C ring (C in Fig. V-3b) and at least lie next to, if not interact with, the rotor (R). It is at connection #1 where the predicted, force-generating interaction between MotB and FliG of the C ring probably occurs. As in *T. primitia*, the bridging density links the stators to the outer, not the inner, rim of the C ring, in line with predictions about the position of FliG upon FliM of the C ring[21]. The C ring dimensions are comparable to those of *Salmonella*[6], but narrower in diameter than *T. primitia*'s (Fig. V-4). It is more bulbous at its bottom, thin in the middle, and wider at its

top. It sits ~ 4 nm below the IM. The bulk of the stator and the rotor (R in Fig. V-3b) is embedded in the membrane and so its borders are indistinguishable from the IM and each other, so no discrete connections are seen between stator and rotor. The edges of these components in Fig. V-4a are conjectured. The *H.g.* rotor is disk-shaped and has a smoother bottom than *Salmonella*'s. Perhaps some loosely bound proteins were removed during the biochemical isolation of *Salmonella*'s basal body to make the rotor's bottom bumpy. The approximate dimensions of the *H.g.* rotor (see Figs. 3b and 4c) are more comparable to *Salmonella*'s isolated basal body than are *T. primitia*'s. The rotor has both a supermembranous S ring and a membrane-embedded M ring, and in *Salmonella*, its respective dimensions are 24 nm and 29 nm[6], while in *T. primitia* they are 24 and 38 nm[7].

From the top of the rotor emerges the rod, which extends through the P ring (P) and presumably the L ring (L), though its density is continuous with the outer membrane (OM) and thus indistinguishable. In individual particles, the OM puckers inward toward the L ring (See Fig. V-2 b–d and Supp. Fig. V-S6), but in the average, the density is spread, presumably by randomly oriented hooks. A novel extended (E) collar lies beside the P ring and above the stator studs. At a more generous density threshold, a peptidoglycan-like density is visible between the membranes and is in line with the E collar (see Supp. Fig. V-S5). The E collar may serve as an additional bushing to aid rotation in the PG layer or as a spacer to prevent crowding of the numerous flagellar motors located at each narrow cell tip.

Below the rotor are two features with high density and low variance but with no noticeable connecting densities: a novel transport (TA) ring and an export mass. The export mass may be a ribosome parked below the rotor feeding flagellin monomers through the TA ring and rotor. The TA ring and export mass may be loosely bound to the C ring or rotor or both because they are absent from the *in vitro* basal body. Both are also present in the reconstructed flagellar motors from *T. primitia* and *Vibrio cholerae* (see Chapter 6) so their presence is not unusual. Many of the flagellar export apparatus proteins are thought to be embedded in the rotor, but FliH, I and J are located in the cytoplasm[22, 23]. FliM and FliN of the C ring bind FliJ and FliH, which in turn bind FliI. FliI is the principal export ATPase and each monomer is 50 kDa and forms a hexameric ring[24]. Assuming typical densities for proteins, were the monomer spherical, it would have a diameter of 5 nm, which is comparable to the TA ring's height. Dividing the ring into six sections, the arc length taken at the radius of the densest TA ring center is 5.5 nm, so it is plausible that the TA ring consists of a hexamer of FliI plus additional bound proteins.

The gap between the rotor and the tip of the inner face of the C ring is 6.5 nm, which is comparable to the 8 nm distance seen in *T. primitia,* but which is approximately three times longer than the ~ 2 nm gap seen in the *in vitro Salmonella* basal body[4] (see star in Fig. V-4a–b). It is believed that the rotor is connected to the C ring by FliG, whose N-terminal domain binds the rotor and whose middle and C-terminal domains bind atop FliM of the C ring[21]. Others place the middle domain on the rotor and have the 2 nm gap spanned by one alpha helix[6], but the gap seems too large in *in situ* motors to be connected that way. The similarity of FliG proteins across species[7] would suggest that

the principle cause of the discrepancy is that without the stators, whatever tether connects rotor and C ring slackens, whereas with the stators, the MotA cytoplasmic domains may push the C ring down and stretch the tether taut (Fig. V-4a–b). Illustrative of this is the manual-fitting of the *Salmonella* basal body[6] into the *H. gracilis* map in Fig. V-5, where the C ring only fit after it was lowered 4 nm from the rotor. Perhaps taut connections are necessary to insure rapid rotation and switching rates.

Methods

Hylemonella gracilis was cultivated from a rotten lily taken from a Caltech pond by placing a drop of liquid upon a 0.22 micron filter resting atop agar containing 10 mM MOPS pH 7. 0 and 0.5 g tryptone and 0.5 g yeast extract per liter. Colonies appeared several weeks later. The 16S rRNA was sequenced from a liquid culture and found to be identical to *Hylemonella gracilis*. Cultures were grown in the above media without MOPS for two days and only reached an O.D. of 0.05. The cells were checked for motility with a light microscope. The cells were then centrifuged and concentrated ten-fold in the same media, then frozen in vitreous ice with a Vitrobot (FEI Company).

Tilt series were collected using a 300 keV FEI Polara FEG TEM automated by UCSF Tomo [25]. The step size was 0.9º and ranged on average from –63º to 60º. The magnification was 34,000 (0.67 nm/pixel) and the total dose was typically ~ 78 $e^-/Å^2$, distributed according to the 1/cos scheme. The nominal defocus was 12 μm. TOMOCTF was used to estimate the experimental defocus by creating a periodogram to which a theoretical CTF was fit[18]. The tilt-series were CTF corrected using phase flipping. The actual defocus ranged from 7.5 μm to 12 μm with a mean of 10 μm (first CTF zero at 4.5 nm). Supplementary Figure V-S1 shows a CTF curve fit to one periodogram. Both the corrected and uncorrected tilt-series were reconstructed and were filtered with a

Gaussian falloff starting either at the first CTF zero or where the experimental CTF amplitude fell below 0.1. The tilt-series were binned two-fold (1.34 nm/pixel) and the tomograms were reconstructed using IMOD [26].

Fifty-nine good motor particles were computationally extracted from fifteen reconstructions in an 88 pixel, cubic volume. All were aligned in reciprocal space to the best-looking particle, using a missing-wedge mask and no object-specific real-space mask, using Bsoft's bfind program[27] and the Peach distributed computing system[28]. Alignments took around a day per particle. Each aligned particle was then refined to each particle to create fifty-nine separate averages, which were then refined to the best-looking average to create a second average, which was oriented upon the z-axis. All particles were then refined to this average to generate a third average. The dominating stator symmetry was visually 13-fold.

Rotational symmetry was detected in two ways. The E collar, P ring, rotor, stator, C ring, and TA ring components were computationally extracted with annular masks. The rotational correlation of the 3-D volumes was computed in real space for all six components of all particles, and from the matrix of coefficients versus angle, a 180 point, 1-D power spectrum was calculated. The individual spectra were then averaged for each component. Only 13-fold symmetry was detected and only in the stator regions. See Supplementary Fig. V-S2. Subsequently, the third average was 13-fold symmetrized, effectively smoothing all other apparently symmetry-less components. This symmetrized average was used as a template to again refine the alignment of all particles to create the final homogeneous average.

Rotational symmetry was also determined using ROTASTAT[19]. 2D images were generated by binning in z certain regions of the third average containing the different motor components. The "background" to which the sample images were compared was

taken from the relatively empty region between the E collar and OM. The rotational symmetry was calculated in reciprocal space and tested for statistical significance. Only the stator regions above and below the membrane had symmetry. The region above showed 11-, 12-, and 13-fold symmetry and the region below showed 12- and 13-fold symmetry. The region above was used to classify particles. Only those particles that displayed strong symmetry (more than 2-fold intensity ratio of foreground to background for a certain symmetry compared to other symmetries) were classified. The 11-fold class had 4 members, the 12-fold 18, the 13-fold 15, and those not strongly symmetric had 22 members. The symmetry of the two stator regions should match, but only 9 of 32 stator-connection predictions were identical to the stator stud region. In order to plot the symmetry of these different classes, the 1-D power spectrum was calculated as above (see Supplementary Fig. V-S2). The 12-fold class had a weaker intensity than the others. The unclassified group also had peak intensity at a symmetry of 13. Separate alignments of the 12- and 13-fold groups were made and symmetrized accordingly. Since the 12-fold group had lower intensity and lacked stator stud features, the homogeneous 13-fold group was focused upon.

In order to determine the resolution, even and odd particles were again separately aligned as above, averaged, and symmetrized 13-fold. The resolution of the entire map, including the variable membrane and cytoplasmic areas, was estimated to be 6.5 nm using the 0.5 criterion of the FSC test. The resolution of the stator and rotor region isolated with a cylindrical mask with a 3-pixel Gaussian falloff edgewidth was 5 nm, so the stator and rotor region probably has a higher resolution than the whole map. CTF correction did not improve the resolution because averages generated from particles taken from the same cells but without corrected tilt-series had the same resolution. In order to determine the statistical significance of features, a 99% confidence interval was calculated (Supplementary Fig. V-S6)[29]. The standard error map for the final

alignment average was generated. The student t-test equation was rearranged so that the true mean lies between two extremes: the experimental mean ± the standard error map times t, whose value for 59 particles for a two-tailed test at a 99% confidence level is 2.662. The extremes were then symmetrized and rescaled to have the same mean and standard deviation as the final structure, then contoured at the same level. Isosurfaces were created and distances measured with Amira (Mercury Computing Systems).

References

1. Kojima, S., and Blair, D. F. The bacterial flagellar motor: structure and function of a complex molecular machine. *Int Rev Cytol*. **233**, 93-134 (2004).
2. Berg, H. C. The rotary motor of bacterial flagella. *Annu Rev Biochem*. **72**, 19-54 (2003).
3. Reid, S. W., et al. The maximum number of torque-generating units in the flagellar motor of Escherichia coli is at least 11. *Proc Natl Acad Sci U S A*. **103**, 8066-71 (2006).
4. Francis, N. R., Sosinsky, G. E., Thomas, D., and DeRosier, D. J. Isolation, characterization and structure of bacterial flagellar motors containing the switch complex. *J Mol Biol*. **235**, 1261-70 (1994).
5. Thomas, D., Morgan, D. G., and DeRosier, D. J. Structures of bacterial flagellar motors from two FliF-FliG gene fusion mutants. *J Bacteriol*. **183**, 6404-12 (2001).

6. Thomas, D. R., Francis, N. R., Xu, C., and DeRosier, D. J. The three-dimensional structure of the flagellar rotor from a clockwise-locked mutant of Salmonella enterica serovar Typhimurium. *J Bacteriol*. **188**, 7039-48 (2006).

7. Murphy, G. E., Leadbetter, J. R., and Jensen, G. J. In situ structure of the complete *Treponema primitia* flagellar motor. *Nature*. **442**, 1062-4 (2006).

8. Sosinsky, G. E., Francis, N. R., Stallmeyer, M. J., and DeRosier, D. J. Substructure of the flagellar basal body of Salmonella typhimurium. *J Mol Biol*. **223**, 171-84 (1992).

9. Stallmeyer, M. J., Hahnenberger, K. M., Sosinsky, G. E., Shapiro, L., and DeRosier, D. J. Image reconstruction of the flagellar basal body of Caulobacter crescentus. *J Mol Biol*. **205**, 511-8 (1989).

10. Suzuki, H., Yonekura, K., and Namba, K. Structure of the rotor of the bacterial flagellar motor revealed by electron cryomicroscopy and single-particle image analysis. *J Mol Biol*. **337**, 105-13 (2004).

11. Young, H. S., Dang, H., Lai, Y., DeRosier, D. J., and Khan, S. Variable symmetry in Salmonella typhimurium flagellar motors. *Biophys J*. **84**, 571-7 (2003).

12. Khan, S., Dapice, M., and Reese, T. S. Effects of mot gene expression on the structure of the flagellar motor. *J Mol Biol*. **202**, 575-84 (1988).

13. Khan, S., Ivey, D. M., and Krulwich, T. A. Membrane ultrastructure of alkaliphilic Bacillus species studied by rapid-freeze electron microscopy. *J Bacteriol*. **174**, 5123-6 (1992).

14. Khan, S., Khan, I. H., and Reese, T. S. New structural features of the flagellar base in Salmonella typhimurium revealed by rapid-freeze electron microscopy. *J Bacteriol*. **173**, 2888-96 (1991).

15. Coulton, J. W., and Murray, R. G. Cell envelope associations of Aquaspirillum serpens flagella. *J Bacteriol*. **136**, 1037-49 (1978).

16. Blair, D. F., and Berg, H. C. Restoration of torque in defective flagellar motors. *Science*. **242**, 1678-81 (1988).

17. Yonekura, K., et al. Electron cryomicroscopic visualization of PomA/B stator units of the sodium-driven flagellar motor in liposomes. *J Mol Biol*. **357**, 73-81 (2006).

18. Fernandez, J. J., Li, S., and Crowther, R. A. CTF determination and correction in electron cryotomography. *Ultramicroscopy*. **106**, 587-96 (2006).

19. Kocsis, E., Cerritelli, M. E., Trus, B. L., Cheng, N., and Steven, A. C. Improved methods for determination of rotational symmetries in macromolecules. *Ultramicroscopy*. **60**, 219-28 (1995).

20. Braun, T. F., Al-Mawsawi, L. Q., Kojima, S., and Blair, D. F. Arrangement of core membrane segments in the MotA/MotB proton-channel complex of Escherichia coli. *Biochemistry*. **43**, 35-45 (2004).

21. Brown, P. N., Terrazas, M., Paul, K., and Blair, D. F. Mutational analysis of the flagellar protein FliG: sites of interaction with FliM and implications for organization of the switch complex. *J Bacteriol*. **189**, 305-12 (2007).

22. Ferris, H. U., and Minamino, T. Flipping the switch: bringing order to flagellar assembly. *Trends Microbiol*. **14**, 519-26 (2006).

23. Gonzalez-Pedrajo, B., Minamino, T., Kihara, M., and Namba, K. Interactions between C ring proteins and export apparatus components: a possible mechanism for facilitating type III protein export. *Mol Microbiol*. **60**, 984-98 (2006).

24. Claret, L., Calder, S. R., Higgins, M., and Hughes, C. Oligomerization and activation of the FliI ATPase central to bacterial flagellum assembly. *Mol Microbiol*. **48**, 1349-55 (2003).

25. Zheng, Q. S., Braunfeld, M. B., Sedat, J. W., and Agard, D. A. An improved strategy for automated electron microscopic tomography. *J Struct Biol*. **147**, 91-101 (2004).

26. Kremer, J. R., Mastronarde, D. N., and McIntosh, J. R. Computer visualization of three-dimensional image data using IMOD. *J Struct Biol*. **116**, 71-6 (1996).

27. Heymann, J. B., and Belnap, D. M. Bsoft: image processing and molecular modeling for electron microscopy. *J Struct Biol*. **157**, 3-18 (2007).

28. Leong, P. A., Heymann, J. B., and Jensen, G. J. Peach: a simple Perl-based system for distributed computation and its application to cryo-EM data processing. *Structure*. **13**, 505-11 (2005).

29. Frank, J. *Three-Dimensional Electron Microscopy of Macromolecular Assemblies.* Oxford University Press, Inc., New York (2006).

Acknowledgements We thank Eric Matson for guiding and performing the identification of the strain. This work was supported in part by NIH grants P01 GM66521 and R01 AI067548 to G.J.J., DOE grant DE-FG02-04ER63785 to G.J.J., a Searle Scholar Award to G.J.J., NSF grant DEB-0321753 to J.R.L., NIH graduate fellowship F31 EB 004179 to G.E.M., and gifts to Caltech from the Ralph M. Parsons Foundation, the Agouron Institute, and the Gordon and Betty Moore Foundation.

Author Contributions G.E.M. collected/analysed the data and drafted the text and figures; J.R.L. provided the cell culture and discourse, E.G.M. identified the species and G.J.J. guided the research and manuscript editing throughout.

Author Information The averaged and symmetrized structure will be deposited in the EM Data Bank (http://www.ebi.ac.uk/msd/index.html).

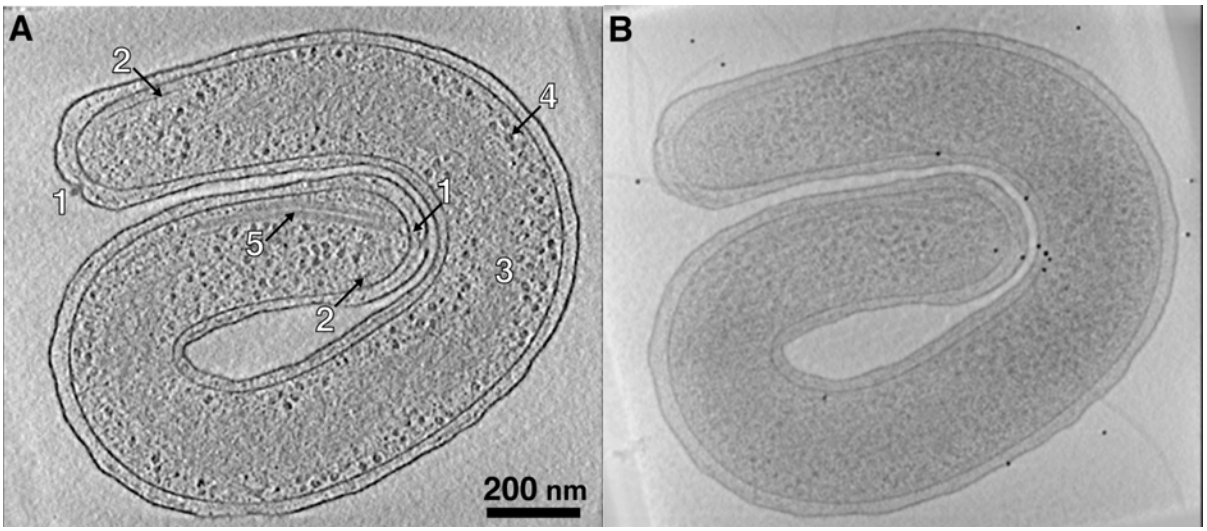

Figure V-1. A reconstructed *H. gracilis* bacteria

A. The flagellar motors (1) are located at the cell tips, as are the chemotaxis arrays (2). A ribosome-excluded region snakes through the middle (3). Ribosome-like particles are more common near the periphery (4). Some cells had flagellar-like filaments in their cytoplasm (5). B. Projection of the whole reconstruction. One to four flagella extend from *H. gracilis'* tip.

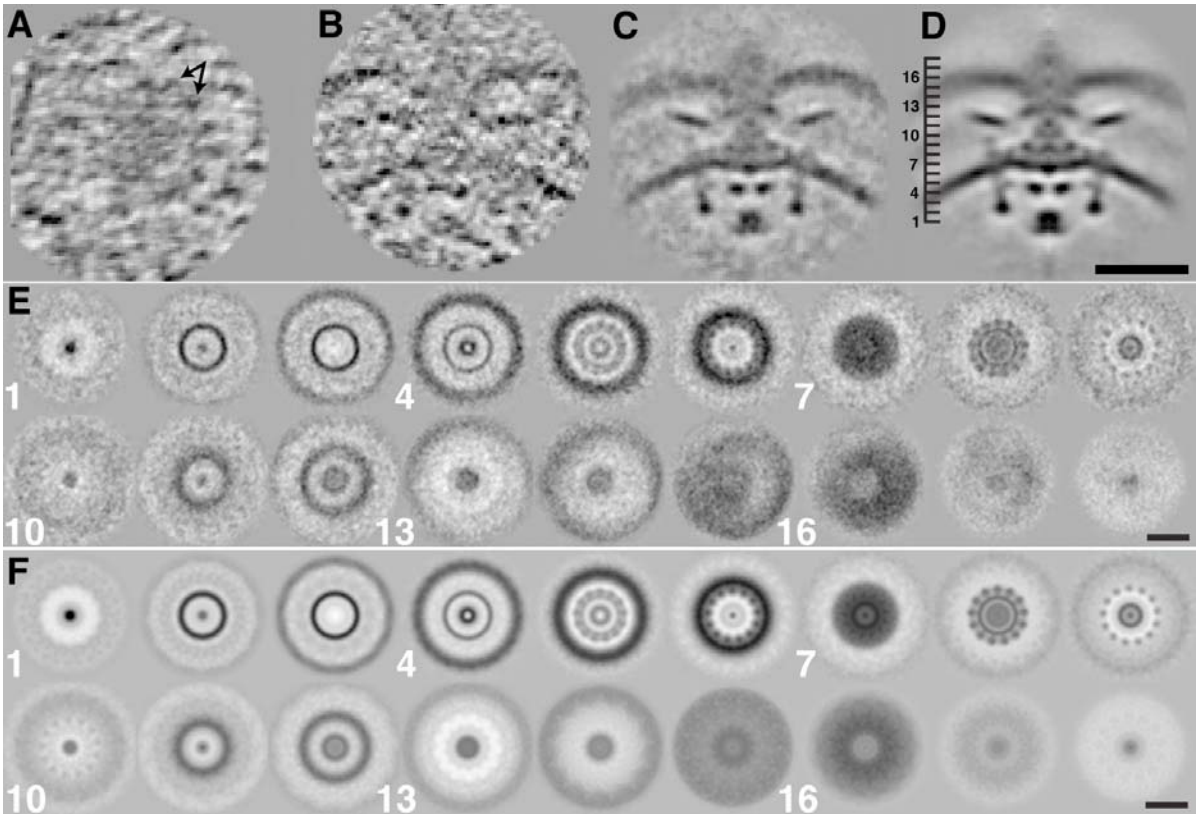

Figure V-2. Sections through the average and 13-fold symmetrization of all particles.

A. Radial section through the stator region of an individual particle at ruler height 8. Arrows point to stator symmetry elements. B. Axial section through another individual particle. C. Axial section through the “homogeneous” mean. D. Symmetrized mean. The sections in panels A through D are 1.34 nm-thick. E. 4 nm-thick serial sections through the mean structure. The numbered slices correspond to the ruler beside panel D. F. 4 nm-thick serial sections through the 13-fold symmetrized mean. (All scale bars are 40 nm.)

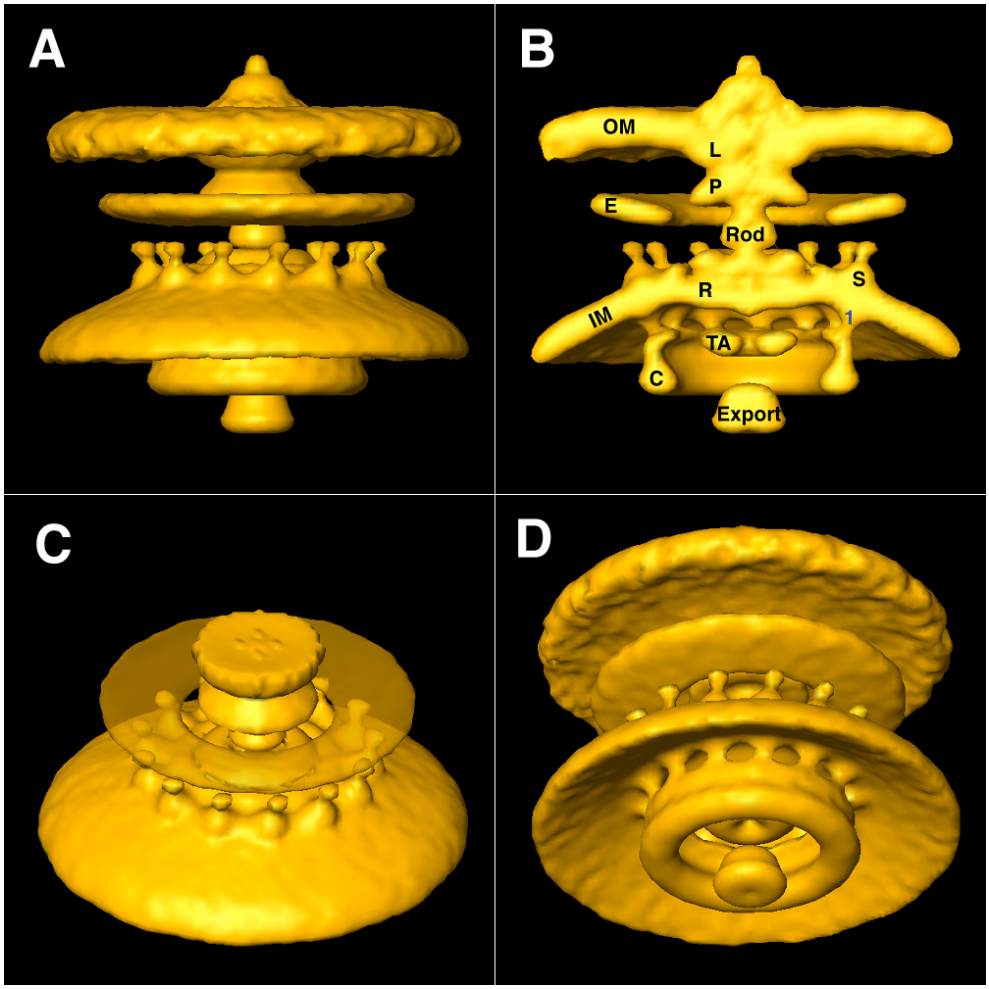

Figure V-3. Isosurface of the averaged and 13-fold symmetrized flagellar motor.

A. View along the membrane. B. Cutaway. The rotor (R) and stators (S) are embedded in the inner membrane (IM) and the C ring (C) connects to the stators through bridging density 1. The rod extends up through the P ring (P) and presumably the L ring (L), though its density is continuous with the outer membrane (OM). The extended collar (E) is novel and lies in the expected plane of the peptidoglycan layer. The transport ring (TA) is also novel and may function in assembly. The export mass may be a ribosome. C. View from the periplasm with the OM removed and the E collar transparent. D. View from the

cytoplasm. Notice that the stator studs and connections are both 13-fold symmetric.

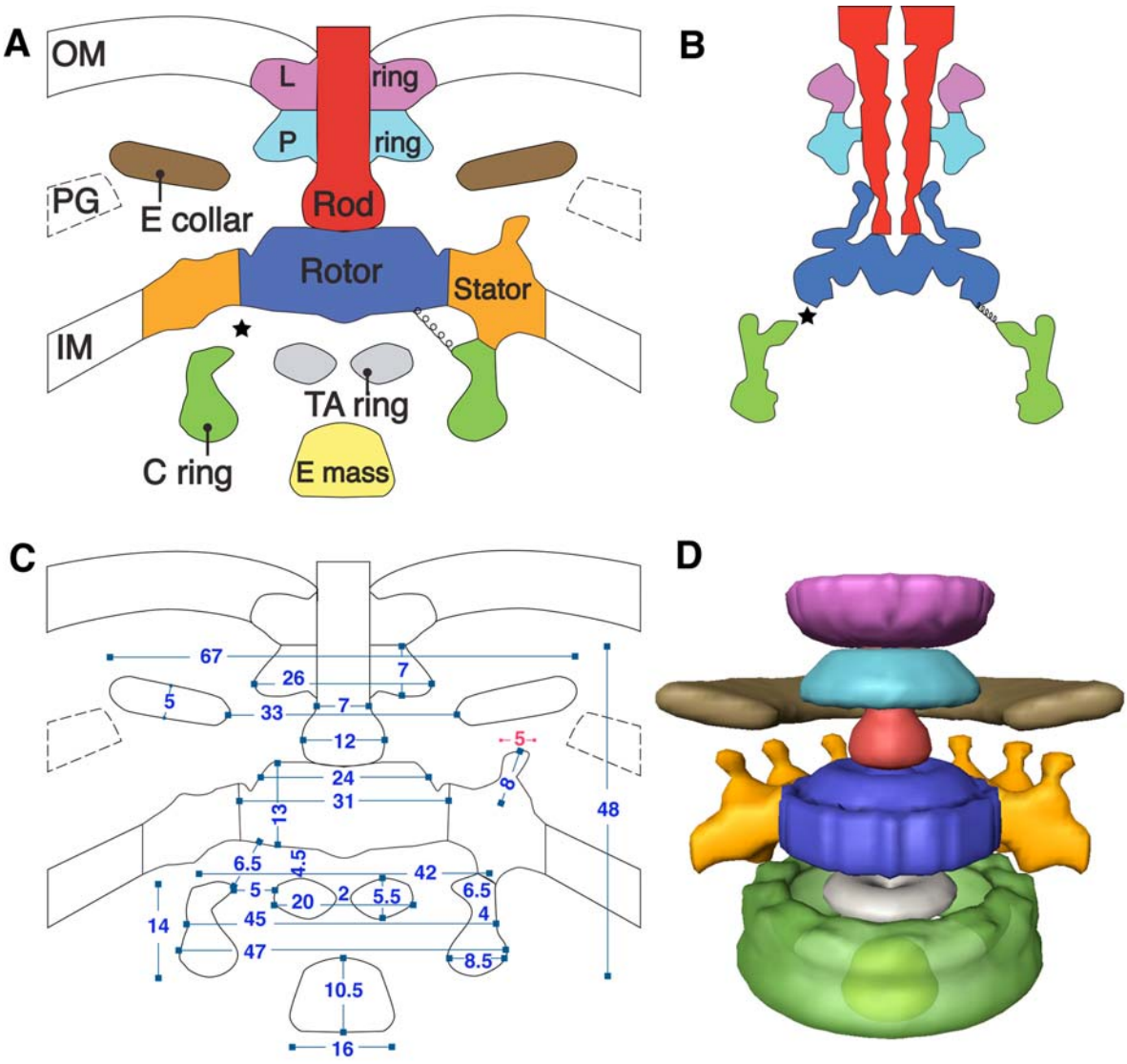

Figure V-4. The components of the flagellar motor

A. Cartoon of the *in situ*, *H. gracilis* motor. The shape of the L ring and the borders of the rotor and stators are conjectured because density was continuous and inseparable from the membranes. B. The similarly colored and scaled motor components of the *in vitro*, *Salmonella* basal body. The starred gap between rotor and C ring is expected to be bridged by some tether, though the gap is about three times longer in the *in situ* motor than the *in vitro* one. C. Measurements of interesting features of the *H. gracilis* motor. The pink

dimension is not to scale, but the stator studs are 5 nm wide. D. The masked-out motor components of the *H. gracilis* map.

Figure V-5. The *Salmonella* basal body fit into *H. gracilis'* motor

The basal body fits plausibly into the *in situ* map only after the C ring is lowered 2.8 nm from the rotor.

Supplementary Information

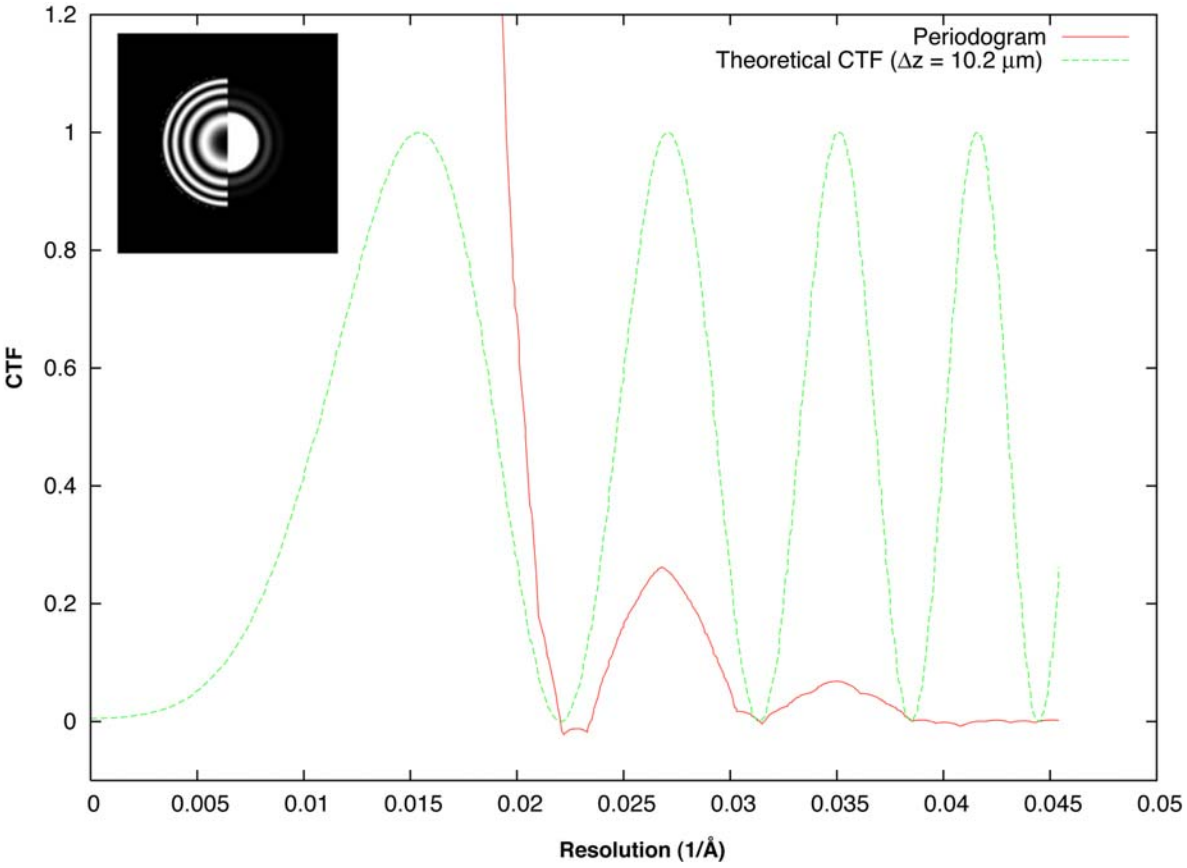

Supplementary Figure V-S1. CTF fitting of a tilt series

From a periodogram generated from a tomographic tilt series, a theoretical CTF curve was fit. The defocus was determined to be 10.2 μm. The information content past the first zero is low, however. The inset shows the theoretical CTF beside the experimental periodogram.

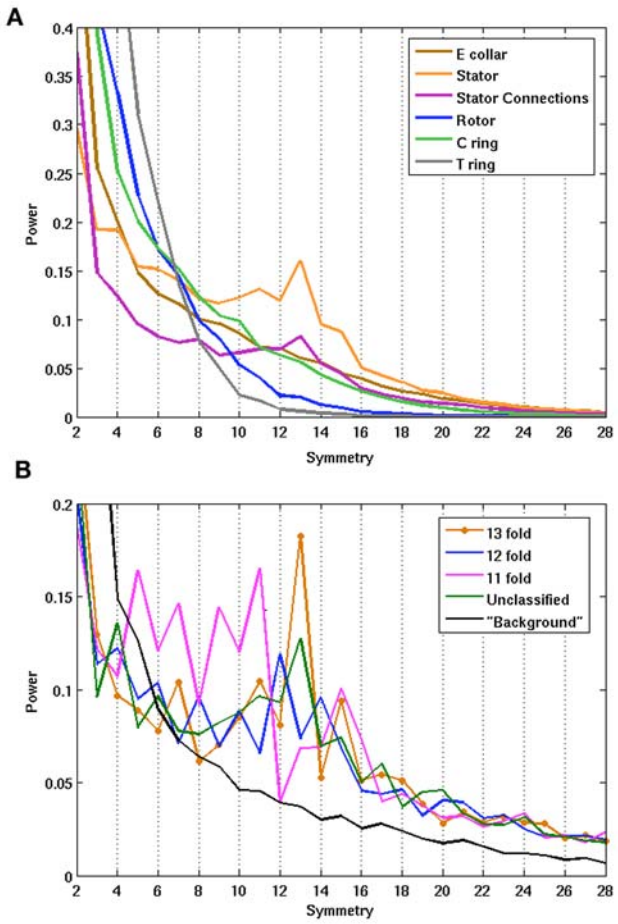

Supplementary Figure V-S2. Rotational power spectrum of motor parts to determine symmetry

A. When the rotational correlation of several excised, 3-D motor regions was calculated in real space, only 13-fold symmetry was detected, and it resided in the stator regions. B. When the rotational power spectrum was calculated in reciprocal space on binned, 2-D images of the same regions using Rotastat, 11-, 12-, and 13-fold symmetry was detected only in the stator regions. The power of the stator stud region from separately classified particles is plotted individually and compared to the power of the “background,” which came from an empty periplasmic region from as many particles. (n.b.: Ordinates are scaled differently.)

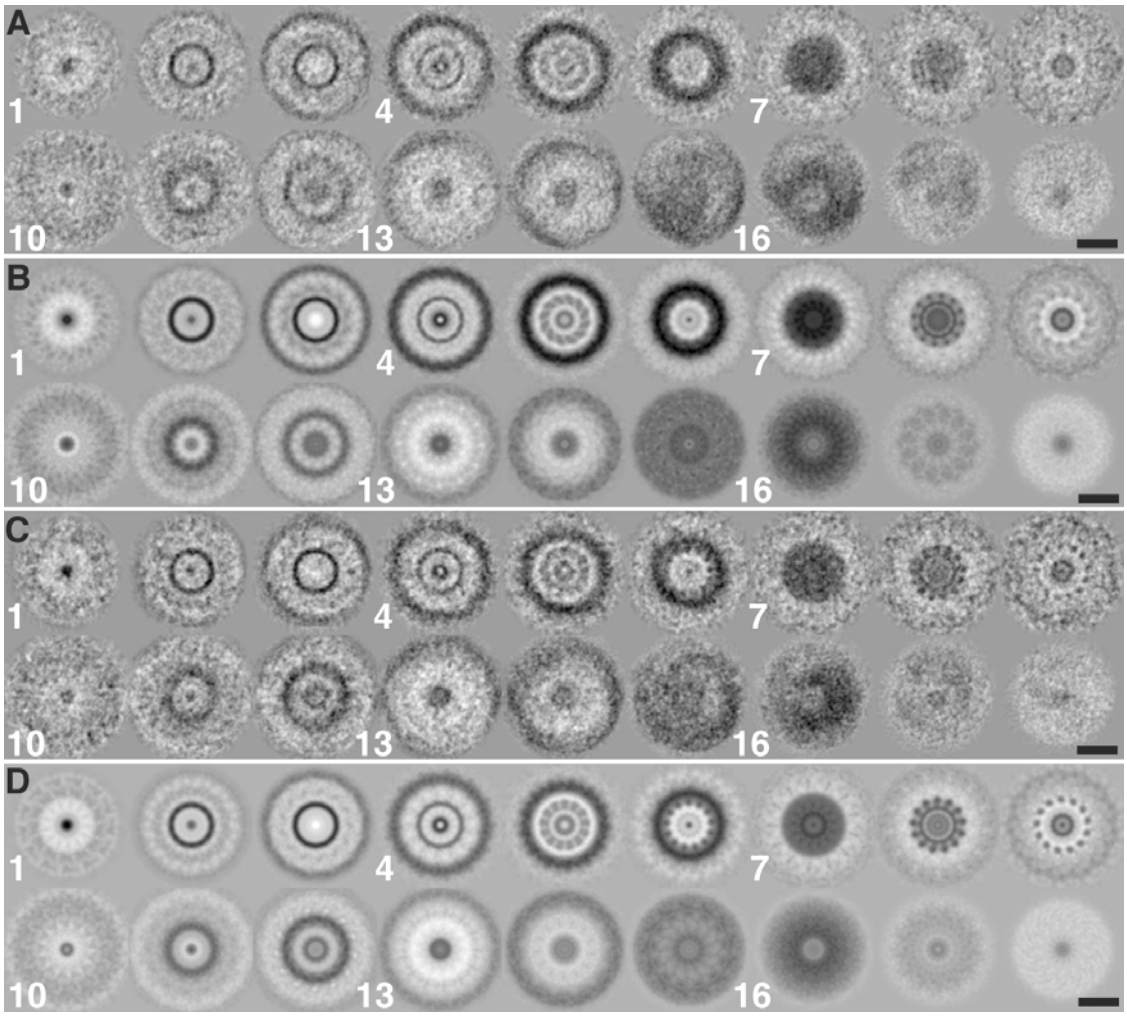

Supplementary Figure V-S3. Serial sections through the 12-fold and 13-fold class means

All sections are 4 nm thick and the numbers correspond to the ruler of Figure V-2 D. A. The 12-fold class mean. B. The 12-fold symmetrized class mean. C. The 13-fold class mean. D. The 13-fold symmetrized class mean. (All scale bars are 40 nm.)

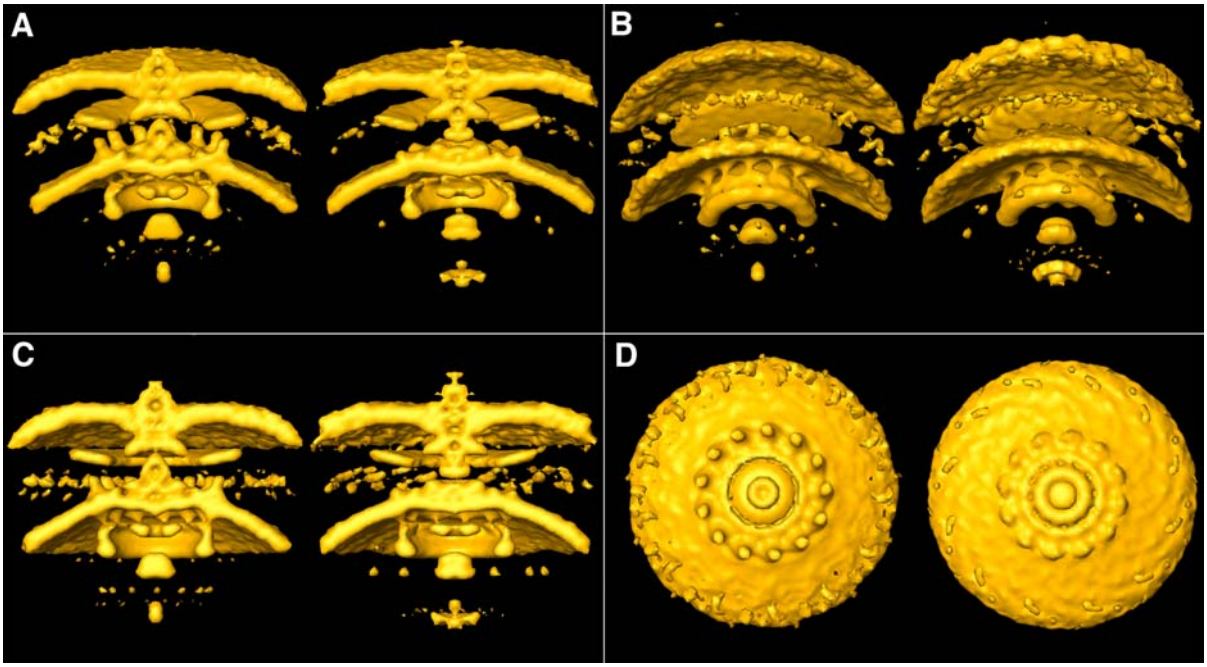

Supplementary Figure V-S4. Comparative isosurfaces of the 13-fold and 12-fold classes

The 13-fold class is on the left, the 12-fold class on the right. A. View from the periplasm. Notice that the 12-fold class lacks as much stator stud density. B. View from the cytoplasm. The respective symmetry is maintained in the stator region both above and below the membrane. C. View along membrane. D. View from above. Notice the pronounced stator stud density in the 13-fold class.

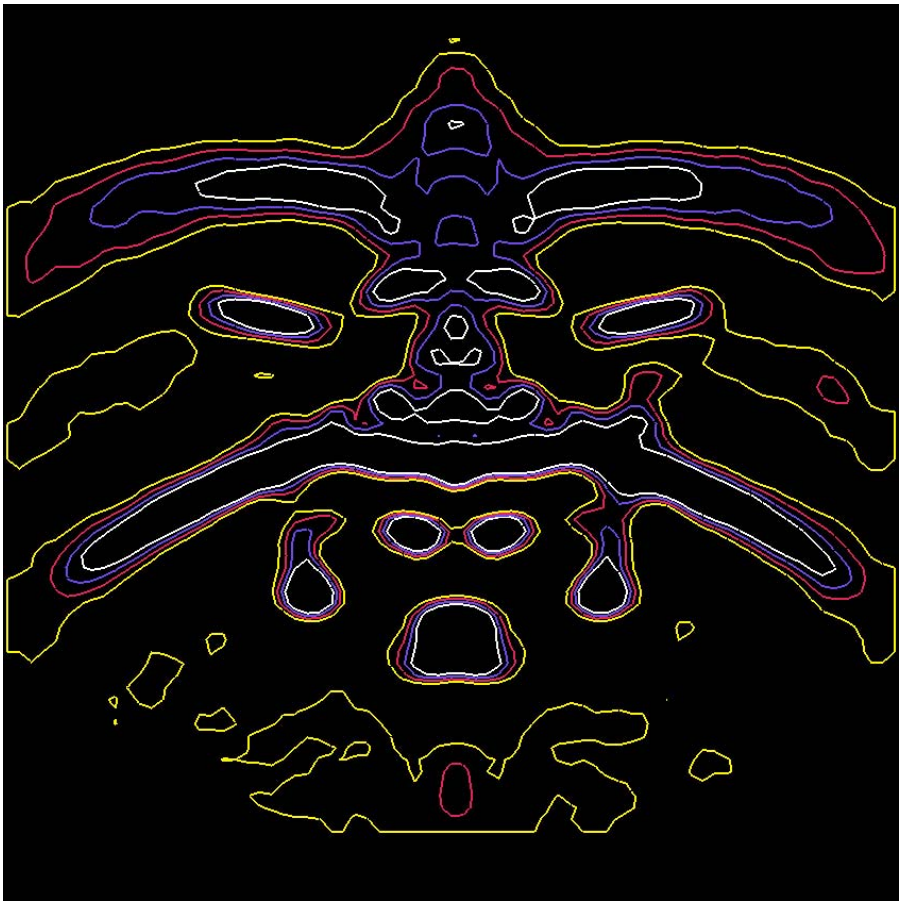

Supplementary Figure V-S5. Isolines of the *H. gracilis* flagellar motor

The high and low densities of the symmetrized mean are represented from white to yellow contours. The red line is the chosen contour for the presented isosurfaces. The blue and white contours are 2 and 3 times less generous in density, and the yellow line is 100% more generous. Notice the density in the PG region contacts the E collar and points towards the stator studs.

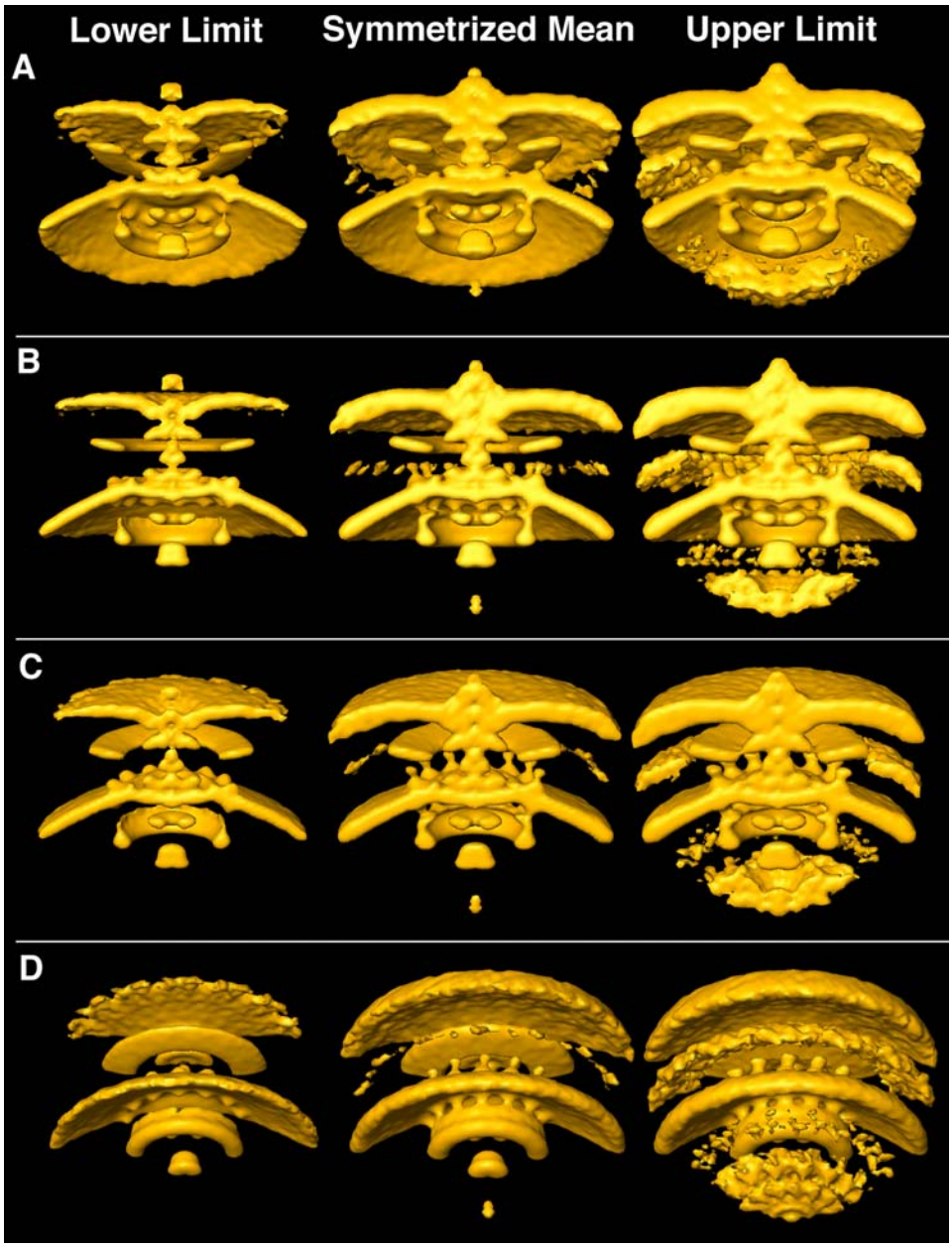

Supplementary Figure V-S6. Statistical confidence interval of the homogeneous final structure

A-D show different views of three maps: the experimental, symmetrized mean and the (subsequently symmetrized) lower and upper limits of the 99% confidence interval. The true mean lies within these limits with the stated confidence.